We are IntechOpen,
the world's leading publisher of
Open Access books
Built by scientists, for scientists

6,900
Open access books available

185,000
International authors and editors

200M
Downloads

154
Countries delivered to

Our authors are among the

TOP 1%
most cited scientists

12.2%
Contributors from top 500 universities

BOOK CITATION INDEX
CLARIVATE ANALYTICS
INDEXED

WEB OF SCIENCE™

Selection of our books indexed in the Book Citation Index
in Web of Science™ Core Collection (BKCI)

Interested in publishing with us?
Contact book.department@intechopen.com

Numbers displayed above are based on latest data collected.
For more information visit www.intechopen.com

Molecular Dynamics Study on Mold and Pattern Breakages in Nanoimprint Lithography

Masaaki Yasuda, Kazuhiro Tada and Yoshihiko Hirai
Osaka Prefecture University
Japan

1. Introduction

Nanoimprint lithography (NIL) is one of the promising technologies for the fabrication of nanostructures at low cost (Chou et al., 1995) (Chou et al., 1996). In NIL, understanding the deformation behaviour of polymer during imprinting processes is an essential issue for high-speed and uniformed fabrication. Since numerical simulations can be efficient approaches for this issue, several studies using continuum mechanics are performed (Hirai et al., 2001) (Hirai et al., 2004) (Song et al., 2008). Continuum mechanics successfully predict the material deformation in submicron scale. However, as the pattern size becomes smaller than several tens of nanometers, continuum mechanics fails to analyze the material behaviour. Single-nanometre resolution has experimentally been demonstrated in NIL (Hua et al., 2004) (Hua et al., 2006). For the exact analysis of the material deformation in nanoscale system, the behaviour of atoms or molecules should be considered.

Molecular dynamics (MD) simulation is a useful tool to study the deformation mechanism of the materials in atomic scale. Several MD studies on NIL process are reported. Kang et al. propose a MD simulation model of a NIL process imprinting an α-quartz stamp into an amorphous poly-(methylmethacrylate) film (Kang et al., 2007). In their study, the distributions of density and stress in the polymer film are calculated for the detail analysis of deformation behaviour. The qualitative agreement between the MD simulation and the experimental data for the density variation of patterned polymer is reported (Woo et al., 2007). Mold geometry effect on springback phenomenon in NIL process is also studied with the MD simulation (Yang et al., 2009).

For metal direct imprinting, more MD studies are performed. Process parameters such as stamp taper angle, imprint depth, temperature and punch velocity are investigated for copper imprinting (Hsu et al., 2004) (Hsu et al., 2005). The mechanism of the atomic-scale friction is studied for aluminium imprinting (Hsieh & Sung, 2007). The metal film thickness effect on pattern formation is also studied (Cheng et al., 2007). Agreement between MD simulation and experimental results is reported for temperature effects on gold imprinting (Hsiung et al., 2009). MD simulation of nanoimprint for alloys is demonstrated (Fang et al., 2007). In order to save computational time, a multi-scale simulation for nanoimprint process that mixes the atomistic and continuum approaches is proposed (Wu & Lin, 2008). Recently, MD simulation of roller nanoimprint process is performed (Wu et al., 2009).

For an exact understanding of the material deformation mechanism during NIL processes, a comprehensive analysis involving three factors should be conducted: mold deformation, processed material deformation and the interaction between them. However, all the MD studies mentioned above treat the mold as a rigid body. Only the deformations of the processed materials are discussed in the studies.

Here, we review our studies on mold and pattern breakages using MD simulation. Firstly, we study the fractures of the independent silicon (Si) mold. The dependences of the Si mold breakages on the crystalline orientation and the defect structures are investigated. Secondly, the fracture mechanism of the pattern is discussed by the MD analysis of the pressure acting on the mold during glass NIL process. Finally, we introduce our resent approaches to investigate the mold deformations in the processed materials during NIL process.

2. Simulation of mold breakages

2.1 Simulation model

As the first step to understand the deformation of the mold during NIL processes, we study the breakages of the independent mold (Tada et al., 2008). Figure 1 shows a configuration of the calculation. The monocrystalline Si mold, which has line and space structures, is pressed onto the rigid substrate without processed materials such as polymers and glasses. The dashed element in Fig. 1 is defined as a unit cell and periodic boundary conditions are applied in the x- and z-directions. The width of the line and space of the mold, the height of the mold pattern and the thickness of the mold base are 3, 9 and 4 nm, respectively. We investigate the crystalline Si molds having two crystalline orientations. Here, we describe the mold which has {110} top surface and {100} front surface as {110}/{100} mold.

The MD simulation is performed using the Tersoff potential (Tersoff, 1988a) (Tersoff, 1988b) to study the mold breakages. The top surface of the mold is moved at a constant velocity of 5 m/s. The initial temperature of the mold is set to be 300 K. Newton's equation of motion is solved using the Verlet algorithm with a time step of 1 fs.
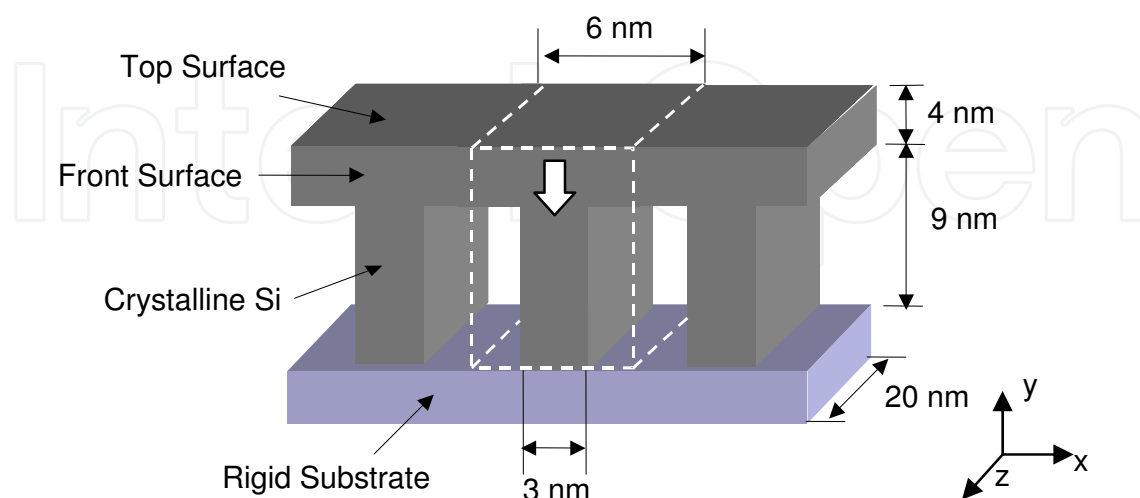

Fig. 1. Configuration of MD simulation for mold breakage analysis. The monocrystalline Si mold is pressed onto the rigid substrate.

2.2 Crystalline orientation dependence on mold breakage

The stress-strain characteristics for {110}/{110} and {110}/{100} molds calculated by the MD simulation are shown in Fig. 2. The compressive strain is calculated as the rate of decrease in the height of the mold. The compressive stress is calculated as the sum of all the atomic forces in the mold top divided by the area of the top surface. The stress increases with an increase in the strain. Yield stresses are 5.5 and 6.7 GPa for {110}/{110} and {110}/{100} molds, respectively.
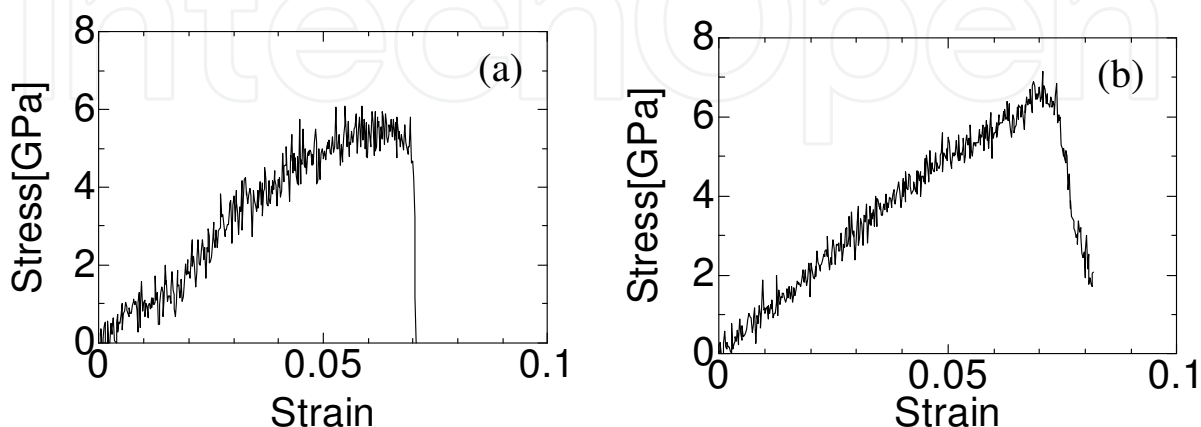
Fig. 2. The stress-strain characteristics for (a) {110}/{110} and (b) {110}/{100} molds.

Figure 3 shows the cross-sectional views at the breaking point for {110}/{110} and {110}/{100} molds. Since the surface energy of {111} crystalline plane is the smallest among those of the other planes, {111} planes could easily slip by shear stress. In {110}/{110} mold, the {111} planes run parallel to the z-direction. This mold could easily fracture along a {111} plane because the width of the mold pattern along the slipping direction is small. In {110}/{100} mold, the {111} planes run parallel to the x-direction. Since the length of the mold pattern along the slipping direction becomes large, the slipping along a {111} plane hardly occurs. Therefore, no slip along a specific crystalline plane is observed in this mold. As a result, {110}/{100} mold exhibits larger strength than {110}/{110} mold. The strength of the mold is strongly associated with the configurations of {111} planes in the mold.
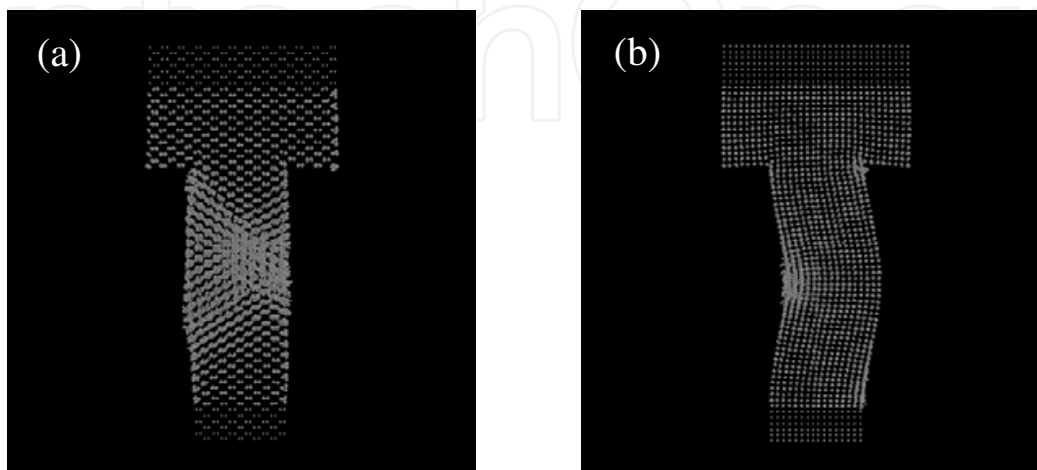

Fig. 3. Cross-sectional views at breaking point for (a) {110}/{110} and (b) {110}/{100} molds.

For comparison, the continuous mechanics simulation using the finite element method is performed. We use the commercially available software MARC distributed by MSC Software. Figure 4 shows the cross-sectional views of the stress distribution calculated by MARC. The aspect ratio of the mold pattern is same as that of MD simulation. Applied pressure is 500 MPa. The compression, shear and von Mises stresses are shown. The maximal stresses are observed at the bottom edge of the mold patterns.
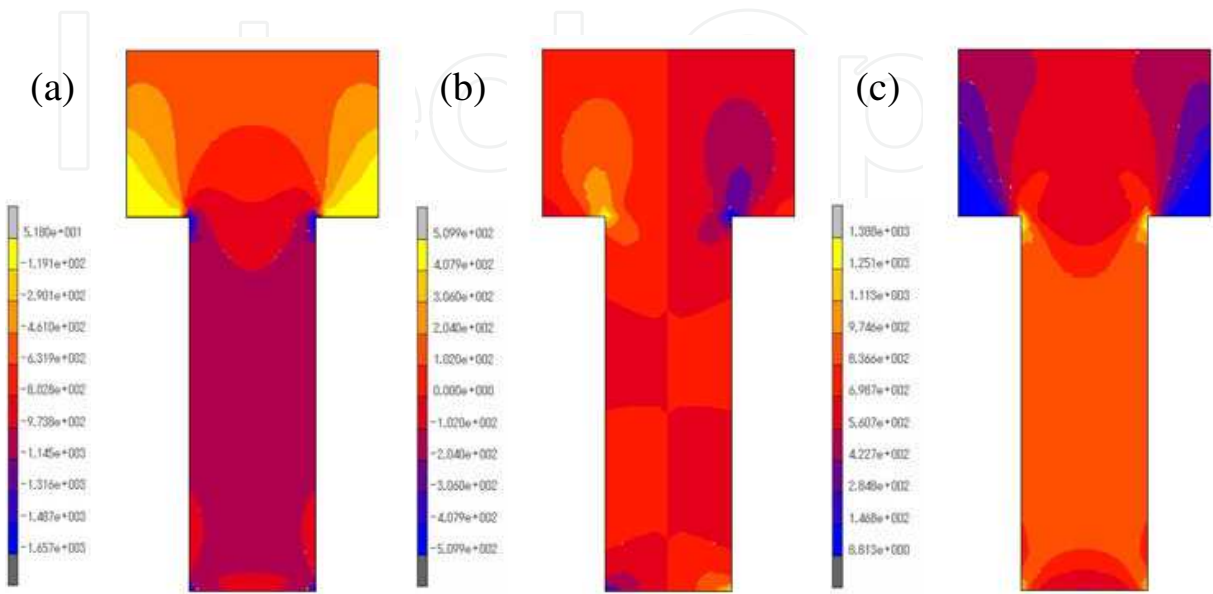

Fig. 4. Stress distributions calculated by the continuum mechanics simulation. (a) compression stress σ_{yy}, (b) shear stress σ_{xy} and (c) von Mises stress.

Figure 5 shows the scanning electron micrograph of the broken pieces of the mold left on the processed material after imprinting. The fracture cross sections of the broken pieces show same crystalline plane orientation. The breakage owing to the slipping of the specific atomic plane is explained by our MD simulation. It is not expected only from the stress distributions obtained by the continuum mechanics simulation.
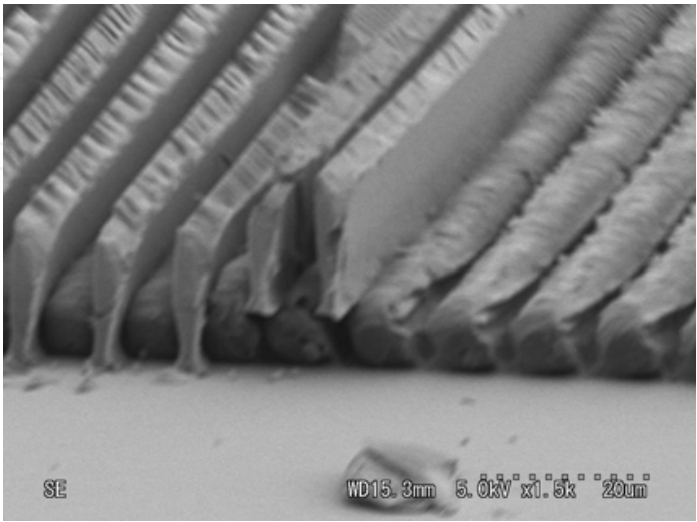

Fig. 5. Scanning electron micrograph of the broken pieces of the mold.

2.3 Breakages of defective mold

The defects caused by the repeated imprinting deteriorate the strength of the mold. Figure 6 shows the cross-sectional views of the stress distributions in {110}/{110} molds with a notch type defect structure during pressing. The mold model has a notch at the center of the mold wall. The depth of the notch is 0.7 nm. The stress is concentrated around the notch defect during pressing as shown in Fig. 6 (a). Finally the mold fractures along {111} plane containing the notch as shown in Fig. 6 (b). The notch acts as a trigger of the crucial mold fracture. Figure 7 shows the stress distribution for {110}/{100} mold. The stress also concentrated around the notch as shown in Fig. 7 (a). The slip along a specific crystalline plane is not observed. However, the notch defect promotes the mold fracture by buckling as shown in Fig. 7 (b).
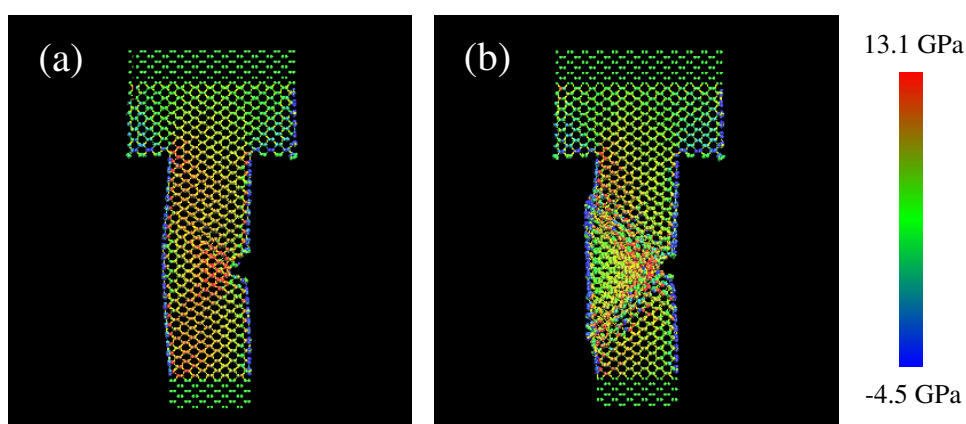

Fig. 6. The stress distributions in {110}/{110} mold with a notch type defect structure (a) before and (b) after mold fracture.
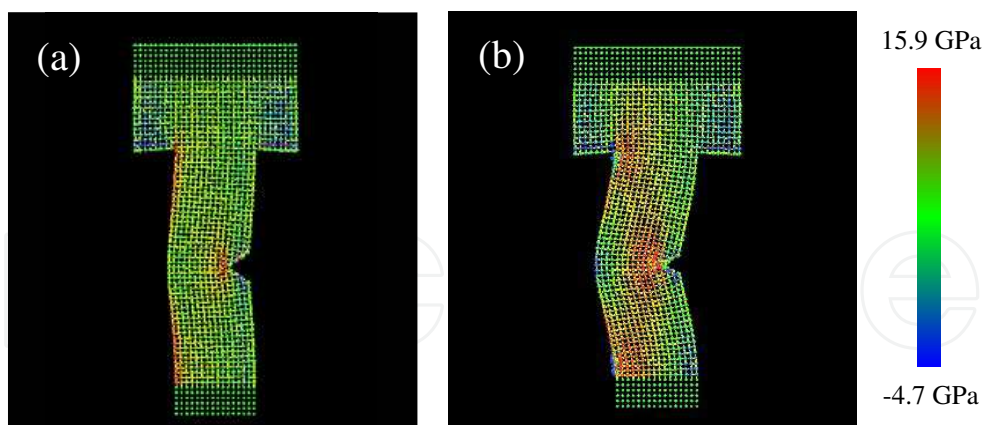

Fig. 7. The stress distributions in {110}/{100} mold with a notch type defect structure (a) before and (b) after mold fracture.

The stress-strain characteristics for {110}/{110} and {110}/{100} molds with a notch type defect structure are shown in Fig. 8. Yield stresses are 4.3 and 4.2 GPa for {110}/{110} and {110}/{100} molds, respectively. These values are smaller than those of the defect-free molds shown in Section 2.2. The strength deterioration of the mold due to the notch defect is more significant for {110}/{100} mold than {110}/{110} mold (Tada et al., 2009a).
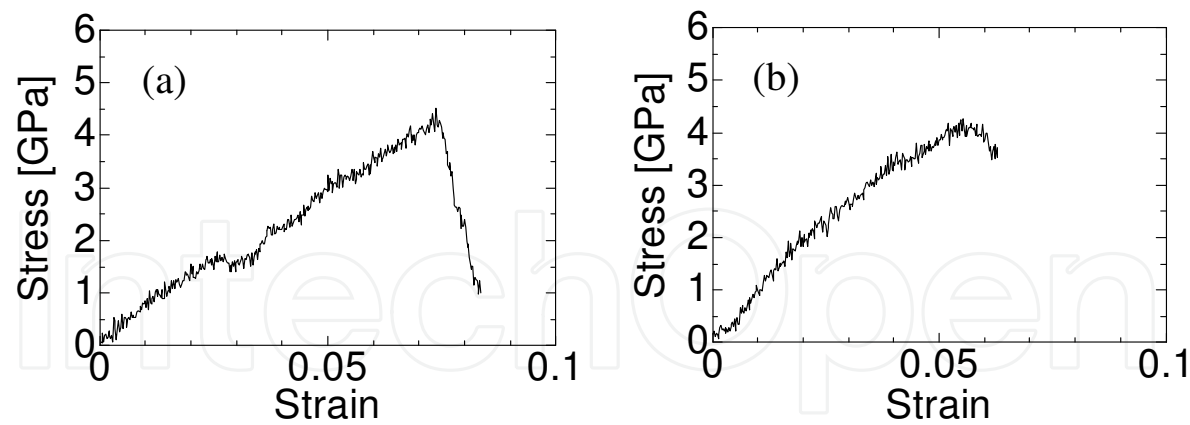
Fig. 8. Stress-strain characteristics for (a) {110}/{110} and (b) {110}/{100} molds with a notch type defect structure.

We also investigate the strength deterioration induced by the vacancy defects. 1.4-nm-diameter spherical vacancies are randomly introduced in the crystalline Si mold. Figure 9 shows the stress distributions in the {110}/{110} mold containing 7 vacancy defects during pressing. Circles in Fig. 9 (a) indicate the positions of the vacancy defects. Before the mold fracture, the stresses around the vacancies are relatively small, because the vacancies act as buffers against compression stress. The fractures along multiple crystalline planes are observed as shown in Fig. 9 (b). Several points where vacancies existed are included in the fracture planes.
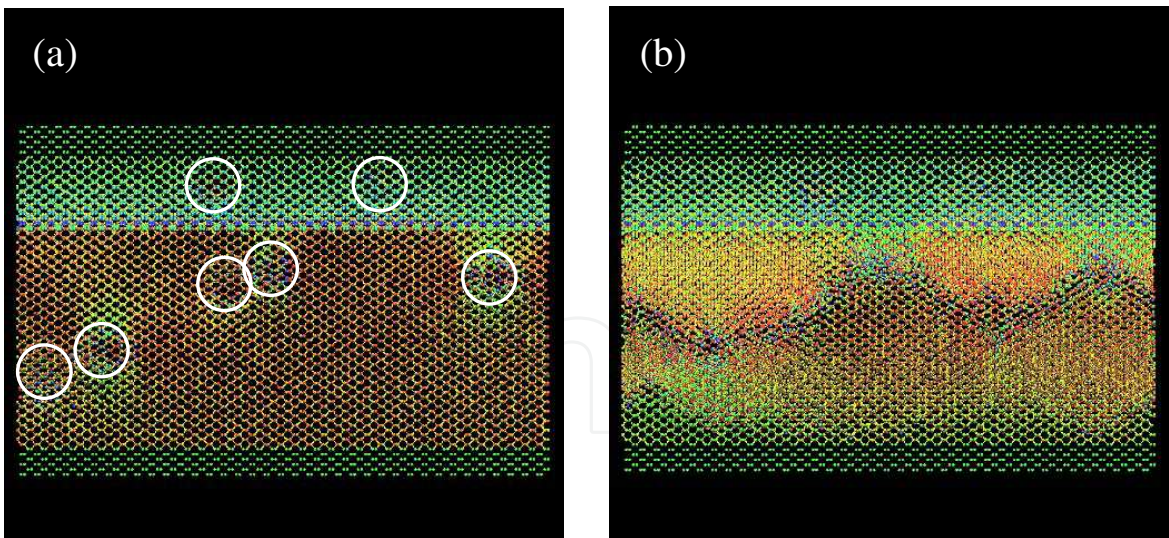

Fig. 9. Stress distributions in y-z plane of the {110}/{110} mold containing 7 vacancy defects (a) before and (b) after mold fracture.

The stress-strain characteristic for {110}/{110} mold containing 7 vacancy defects during pressing is shown in Fig. 10. The stress decreases more gradually after fracture than that of defect-free mold. This gradual decrease of the stress is attributed to the fractures along multiple crystalline planes. Yield stress is 5.3 GPa. The strength deterioration due to the vacancy defects is smaller than that due to the notch defects. The vacancy defects do not act

as a trigger of the crucial mold fracture. These results indicate that the surface defects on the mold sidewall such as notches become more serious causes of the mold breakage than the defects originally contained in the mold material, such as vacancies.
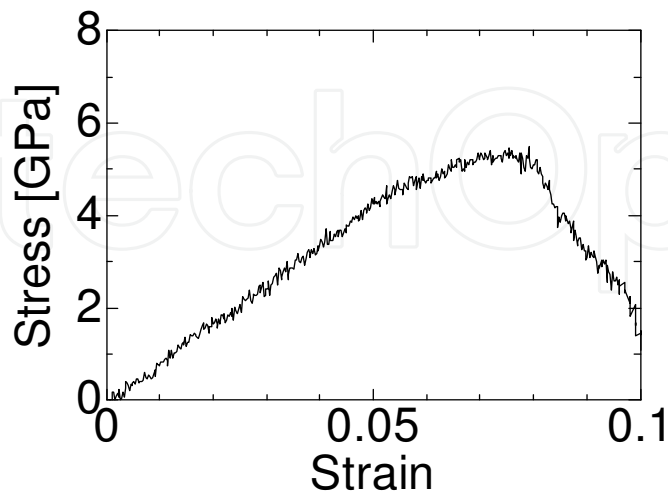

Fig. 10. Stress-strain characteristics for {110}/{110} mold containing 7 vacancy defects.

3. Simulation of pattern breakages

3.1 Simulation model

In this section, we discuss the pattern breakages in NIL. While polymer materials are often used as resist materials in NIL, inorganic glasses are also promising materials for optical devises (Hirai et al., 2003) (Okinaka et al., 2006) (Akita et al., 2007). However, it is more difficult to fabricate nanostructures on glass materials than on polymer materials because of the fragility of glass. Here, we investigate the glass deformation in NIL with a MD simulation.

Figure 11 shows a schematic diagram of the calculation system. The monocrystalline Si mold, which has line and space structures, is pressed onto the SiO_2 glass film. Si mold is treated as a rigid body. We define the dashed element in Fig. 11 as a unit cell. Periodic boundary conditions are applied in the x- and z-directions. 5 nm width and 2 nm thickness are considered as a unit cell in the x- and z-directions, respectively. The height of the mold pattern and the thickness of the glass film are 2.5 and 5 nm, respectively. 1-nm-thick bottom region in SiO_2 glass film is assumed to be rigid as a substrate.

Melt-quench method is used to form the initial structures of the SiO_2 glass by the MD simulation (Delaye et al., 1997). The SiO_2 crystal is melted and rapidly quenched from 8500 to 2500 K at a rate of 5×10^{15} K/s and from 2500 to 300 K at 5×10^{14} K/s to become SiO_2 glass.

Born-Mayer-Huggins potential is adopted to describe the interactions between atoms in the SiO_2 glass (Delaye et al., 1997). Morse potential is used to simulate the interaction between a Si mold and SiO_2 glass (Takada et al., 2004). The mold is pressed and released from glass at a constant velocity of 50 m/s. The temperature of the glass is maintained at 1500 K during the mold pressing using the velocity-scaling method. After filling the cavity of the mold with glass, the system is cooled to 300 K. Finally, the mold is released from the glass.
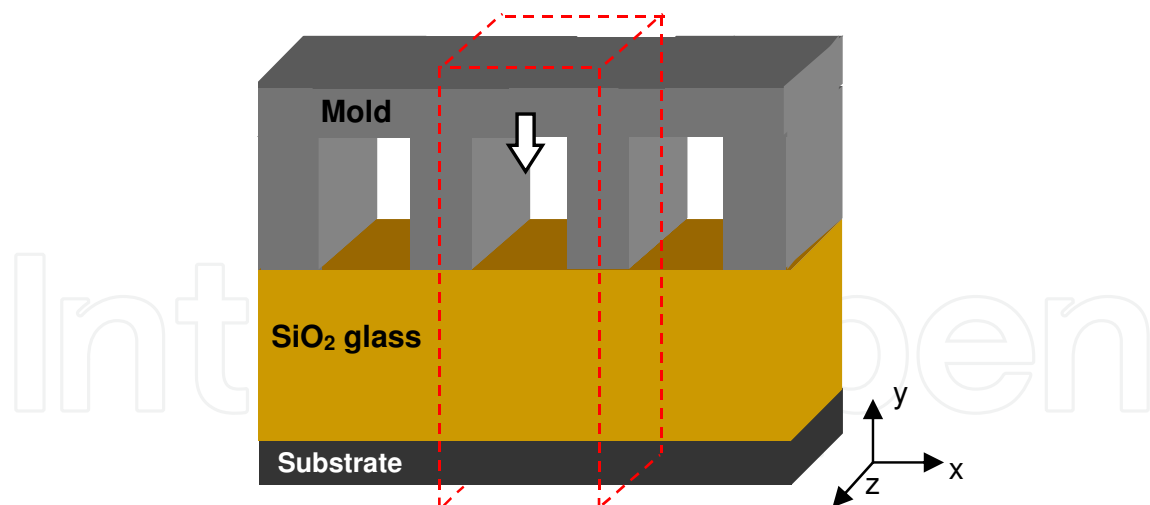
Fig. 11. Schematic diagram of the calculation system. The rigid Si mold, which has line and space structures, is pressed onto the SiO$_2$ glass film.

3.2 Glass nanoimprint process

Figure 12 shows the variation of the pressure acting on the mold versus mold position obtained by the simulation (Tada et al., 2009b). The cross-sectional views of each step are also shown. The pressure acting on the mold is calculated as the sum of all the atomic forces on the mold divided by the area of the top surface. The position where the mold contacts the glass is 0 nm. Initially, the pressure increases linearly as the mold is pressed to the glass [region (a) to (b)]. In this region, elastic deformation is dominant. In the region where the pressure increases nonlinearly, the plastic flow of the glass to the cavity of the mold is observed [region (b)]. Because of the highly viscous flow above the glass transition temperature, the glass does not fracture in this plastic flow. After filling the cavity with glass, the system is relaxed by resting the mold [region (c)]. During the cooling process the pressure decreases due to the stress relaxation. Then, the mold is released from the glass. Elastic recovery is observed in the first stage of releasing [region (c) to (d)]. The pressure acting on the mold shows a negative value since the tension force acts in the glass by adhesion between the glass and the mold [region (d) to (f)]. Finally, the mold is exfoliated from the mold. The pressure acting on the mold largely disappears [region (e)]. A fluctuation in pressure is observed until the mold is completely released from the glass [region (e) to (f)]. This fluctuation in pressure shows the stick slip phenomena between the side wall of the mold and the glass. The height of the glass after the mold separation [region (f)] is larger than that at the mold holding process [region (c)]. The springback phenomenon is observed. After the mold releasing, the segmentalization is observed at the surface region of the glass.

From our simulation, it is found that the pressure to fill the cavity depends on the glass thickness. If the cavity width and depth are constant, the filling pressure increases as the glass thickness decreases. Because the glass is fixed to the substrate, the mobility of the glass near the substrate is low. Therefore, the thinner glass is hardly deformed. Filling pressure also depends on the cavity width. If the cavity depth and the glass thickness are constant, the pressure increases as the cavity width decreases. These results are consistent with that obtained by the continuous mechanics (Hirai et al., 2004).
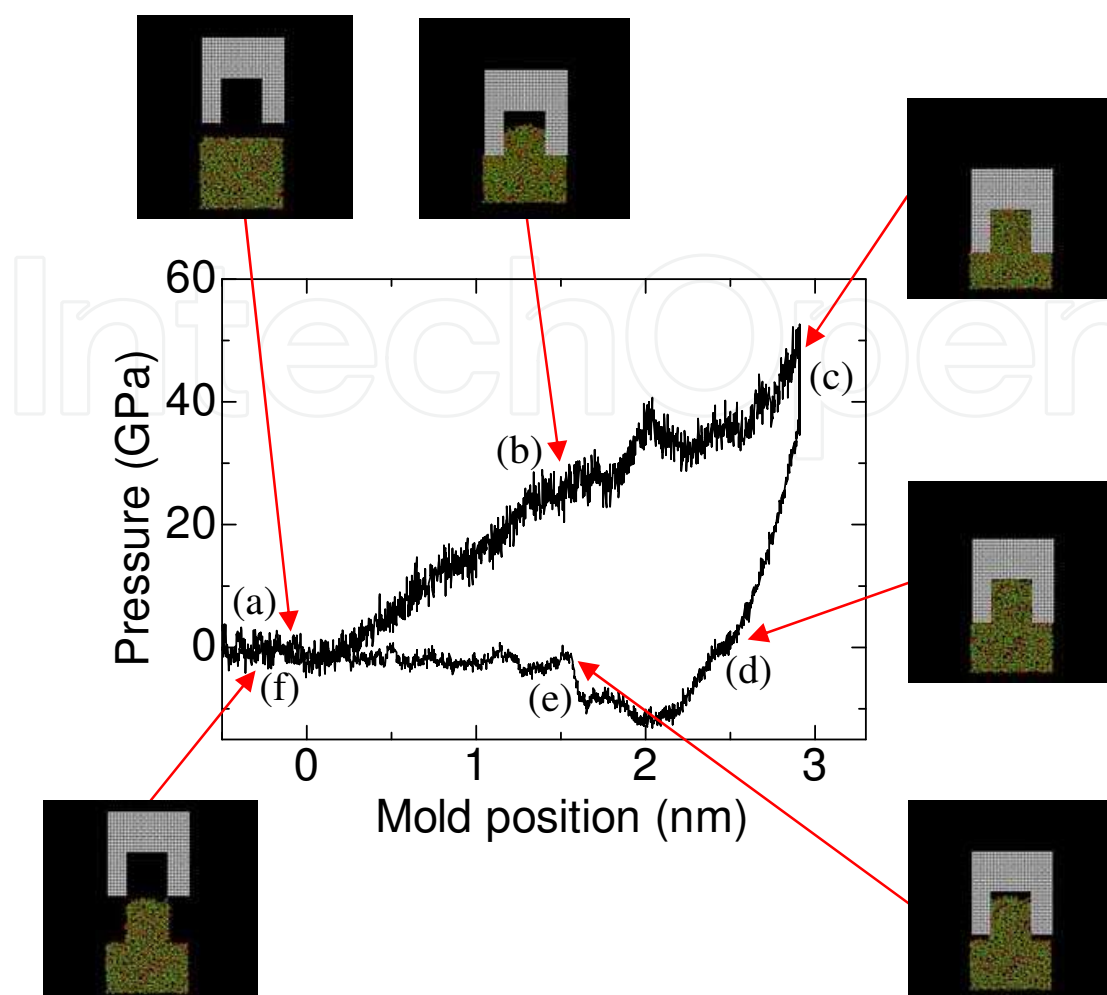
Fig. 12. The variation of the pressure acting on the mold versus mold position.

Kang et al. divided the polymer into three regions to analyze the adhesion and friction forces between the mold and the polymer in detail (Kang et al., 2007). In order to perform the same analysis, we divide the glass into three regions as shown in Fig. 13 (a). The variations of the pressure acting on the mold by regions 1, 2 and 3 versus mold position are shown in Figs. 13 (b), (c) and (d), respectively. During the mold pressing, the pressure from the region 1 mainly acts on the mold. Large compressive stress is concentrated under the protruding portion of the mold. The pressure from the region 2 begins to act at the mold position of 15 nm. This indicates that the glass does not flow into mold cavity soon after the mold pressing starts. At that point, a shear stress arises in the glass. This shear stress reflects the pressure increase in the region 3. During the mold releasing, the pressure acting on the mold is contributed by the regions 1 and 2. The contribution by the region 1 is the adhesion force between the top surface of the mold and the glass. The contribution by the region 2 is the friction force between the side wall of the mold and the glass. A fluctuation in pressure is observed only in the region 2. This indicates that the fluctuation in total pressure shown in Fig. 12 is attributed to the stick slip phenomena between the side wall of the mold and the glass. The contribution by the region 3 is smaller than those by regions 1 and 2 during whole NIL process. The result shown in Fig. 13 is similar to that reported for polymer imprinting (Kang et al., 2007).
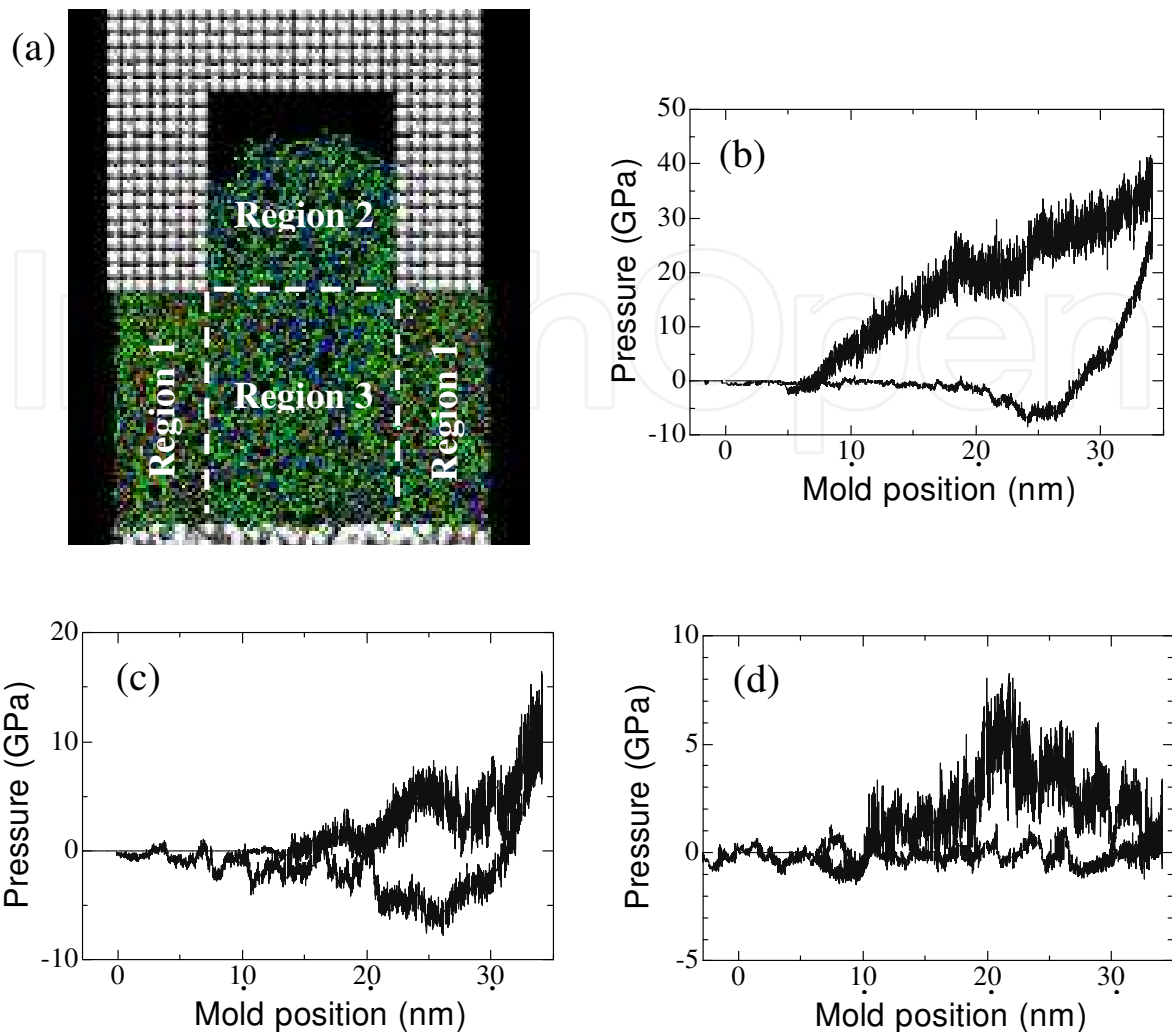
Fig. 13. The variations of the pressure acting on the mold by (a) divided glass regions. The pressures by (b) region 1, (c) region 2 and (d) region 3 are separately analyzed.

3.3 Glass pattern breakages

As discussed in Section 3.2, the friction force appears between the side wall of the mold and the glass during the mold releasing. This friction force induces stretching of the glass. Since the friction force between the side wall of the mold and the glass depends on the contact area, the maximum friction force becomes large for the high aspect ratio pattern (Kang et al., 2007). If the depth of the mold cavity is constant, the maximum tensile stress in the glass increases with the decrease in the cavity width (Tada et al., 2009c). Figure 14 shows the cross-sectional views of the glass pattern after the mold releasing obtained by the MD simulation. The depth of the mold cavity is 2.5 nm. When the cavity width is 2 nm, the pattern is successfully transferred in the glass as shown in Fig. 14 (a). However, for the cavity width of 1 nm, narrow line grass pattern fractures during the mold releasing as shown in Fig. 14 (b). The tension stress induced by the friction force is concentrated at the narrow grass pattern. This is because the minimum line width for the successful pattern transfer depends on the mold geometry. From the MD study, the ultimate resolution in the SiO_2 glass NIL was estimated to be 0.4 nm (Tada et al., 2009c).
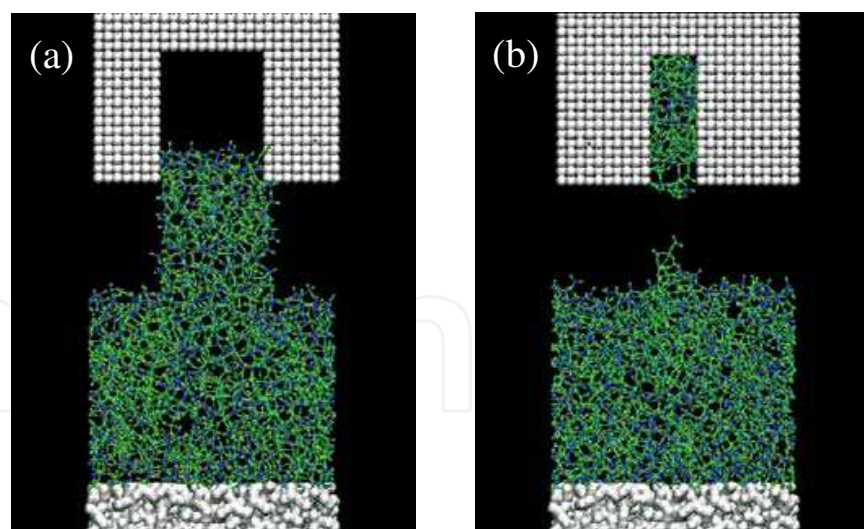
Fig. 14. The cross-sectional views of the glass pattern after the mold releasing. The cavity widths are (a) 2 and (b) 1 nm.

4. Mold deformation in NIL process

Finally, we study the mold deformation in NIL process with the MD simulation. In Sections 2 and 3, either the mold or the processed material is treated as a rigid body. In this section, deformations of both the mold and the processed material are investigated simultaneously.

The configuration of the simulation is almost same as that shown in Fig. 11. However, the Si mold is not treated as a rigid body. The motion of atoms in the mold is also calculated using the Tersoff potential (Tersoff, 1988a) (Tersoff, 1988b). In this simulation, the processed material is the pseudo-glass. For the calculation of the pseudo-glass deformation, we use the Born-Mayer-Huggins potential for SiO_2 glass (Delaye et al., 1997). The potential parameter for pseudo-glass is changed to make Young's modulus smaller (6 GPa) for the NIL process using Si mold. In order to calculate the interaction between a Si mold and SiO_2 glass Lennard-Jones potential is used.

The top surface of the mold is pressed onto the pseudo-glass at a constant speed of 50 m/s. Periodic boundary conditions are applied in the x- and z- directions. The size of a unit cell in the mold structure is 2.7 nm wide, 5.0 nm high and 2.0 nm deep. The thickness of the mold basement is 1.5 nm. The few upper and bottom atomic layers are fixed. The initial temperature of the simulation is 300 K.

Figure 15 shows the cross-sectional views of the stress distributions in {110}/{100} mold during pressing. The maximum stress is concentrated on the sidewall of the Si mold until whole the protruding portion of the mold is buried in the glass as shown in Figs. 15 (a) and (b). Further pressing raises the stress inside the mold as shown in Fig. 15 (c).

Figure 16 shows the cross-sectional views of the stress distributions in {110}/{110} mold during pressing. At the beginning of the pressing process, the relatively large stress is observed at a contact area and the side wall of the mold as shown in Fig. 16 (a). In this case, the mold begins to bend in process of pressing as shown in Fig. 16 (b). The maximum stress concentrates around the bottom edge of the mold with the progress of bending as shown in Fig. 16 (c). Because of the periodic boundary condition in x-direstion, the head of the mold appears from the opposite side of the structure in Fig. 16 (c).
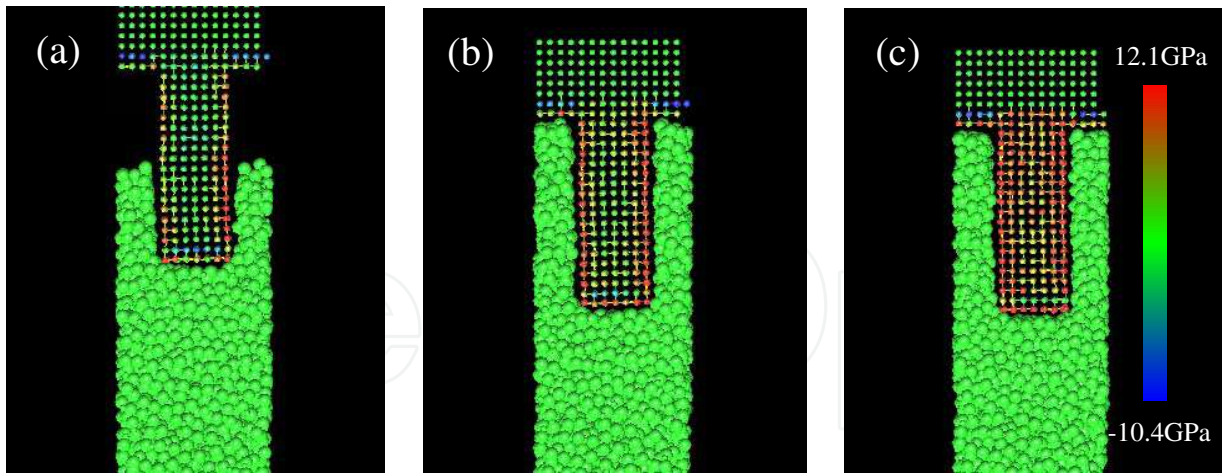
Fig. 15. The cross-sectional views of the stress distributions in {110}/{100} mold during pseudo-glass imprinting.
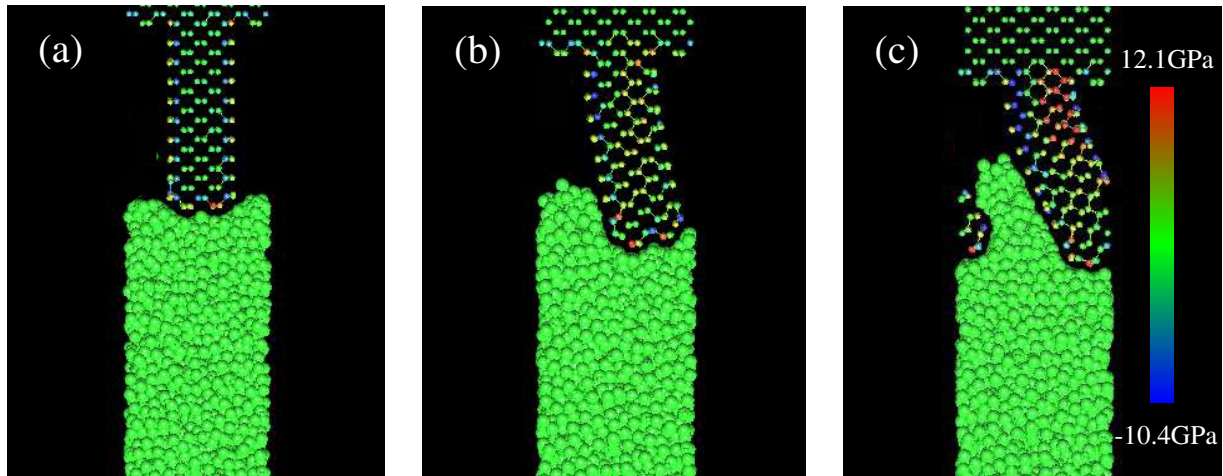

Fig. 16. The cross-sectional views of the stress distributions in {110}/{110} mold during pseudo-glass imprinting.

5. Conclusion

The MD simulations are performed to investigate the mechanism of the mold and the pattern breakages. From the analysis of the independent mold, the dependences of the mold strength on the crystal orientation and the defect structure are revealed. The analysis of the pressure acting on the mold indicates that the frictions between the mold sidewall and the processed material induce the pattern stretching and breakages. The simulation of the mold deformation during NIL process reveals that the excessive pressing or the bending of the mold induces the abnormal stress in the mold, which is the possible cause of the mold breakage.

The breakages of the mold and the pattern largely depend on the surface condition of the materials. Our MD simulations do not consider the anti-sticking treatment and surface geometry such as surface roughness. These are the important future subjects for the MD study of NIL process.

6. Acknowledgement

7. References

Akita, Y.; Watanabe, T.; Hara, W.; Matsuda, A. & Yoshimoto, M. (2007). Fine pattern fabrication on glass surface by imprint lithography, *Jpn. J. Appl. Phys.,* Vol. 46, Nos. 12-16, (April 2007) pp. L342-L344

Cheng, M. –C.; Hsiung, H. –Y.; Lu, Y. –T. & Sung, C. –K. (2007b). The effect of metal-film thickness on pattern formation by using direct imprint, *Jpn. J. Appl. Phys.,* Vol. 46, No. 9B, (September 2007) pp. 6382-6386

Chou, S. Y.; Krauss, P. R. & Renstrom, P. J. (1995). Imprint of sub-25 nm vias and trenches in polymers, *Appl. Phys. Lett.,* Vol. 67, No. 21, (November 1995) pp. 3114-3116

Chou, S. Y.; Krauss, P. R. & Renstrom, P. J. (1996). Imprint lithography with 25-nanometer resolution, *Science,* Vol. 272, No. 5258, (April 1996) pp. 85-87

Delaye, J. M.; Louis-Achille, V. & Ghaleb, D. (1997). Modelling oxide glasses with Born–Mayer–Huggins potentials: Effect of composition on structural changes, *J. Non-Cryst. Solids,* Vol. 210, Nos. 2-3, (March 1997) pp. 232-242

Fang, T. –H.; Wu, C. -D. & Chang, W. –J. (2007). Molecular dynamics analysis of nanoimprinted Cu–Ni alloys, *Appl. Surf. Sci.,* Vol. 253, No. 16 (June 2007) pp. 6963-6968

Hsieh, C. –W. & Sung, C. –K. (2007). Atomic-scale friction in direct imprinting process: Molecular dynamics simulation, *Jpn. J. Appl. Phys.,* Vol. 46, No. 9B, (September 2007) pp. 6387-6390

Hsiung, H. Y.; Chen, H. Y. & Sun, C. K. (2009). Temperature effects on formation of metallic patterns in direct nanoimprint technique - Molecular dynamics simulation and experiment, *J. Mater. Process. Tech.,* Vol. 209, No. 9, (May 2009) pp. 4223-4626

Hsu, Q. –C.; Wu, C. –D. & Fang, T. –H. (2004). Deformation mechanism and punch taper effects on nanoimprint process by molecular dynamics, *Jpn. J. Appl. Phys.,* Vol. 43, No. 11A, (November 2004) pp. 7665-7669

Hsu, Q. –C.; Wu, C. –D. & Fang, T. –H. (2005). Studies on nanoimprint process parameters of copper by molecular dynamics analysis, *Comput. Mater. Sci.,* Vol. 34, No. 4, (December 2005) pp. 314-322

Hirai, Y.; Kanakugi, K.; Yamaguchi, T.; Yao, K.; Kitagawa, S. & Tanaka, Y. (2003). Fine pattern fabrication on glass surface by imprint lithography, *Microelectron. Eng.,* Vols. 67-68, (June 2003) pp. 237-244

Hirai, Y.; Fujiwara, M.; Okuno, T.; Tanaka, Y.; Endo, M.; Irie, S.; Nakagawa, K. & Sasago, M. (2004). Study of the resist deformation in nanoimprint lithography, *J. Vac. Sci. Technol. B,* Vol. 19, No. 6, (Novemver 2001) pp. 2811-2815

Hirai, Y.; Konishi, T.; Yoshikawa, T. & Yoshida, S. (2004). Simulation and experimental study of polymer deformation in nanoimprint lithography, *J. Vac. Sci. Technol. B,* Vol. 22, No. 6, (Novemver 2004) pp. 3288-3293

Hua, F.; Sun, Y.; Gaur, A.; Meitl, M. A.; Bilhaut, L.; Rotkina, L.; Wang, J.; Geil, P.; Shim, M.; Rogers, J. A. & Shim, A. (2004). Polymer imprint lithography with molecular-scale resolution, *Nano Lett.,* Vol. 4, No. 12, (December 2004) pp. 2467-2471

Hua, F.; Gaur, A.; Sun, Y.; Word, M.; Jin, N.; Adesida, I.; Shim, M.; Shim, A. & Rogers, J. A. (2006). Processing dependent behaviour of soft imprint lithography on the 1-10-nm scale, *IEEE Trans. Nanotechnol.,* Vol. 5, No. 3, (May 2006) pp. 301-308

Kang, J. -H.; Kim, K. –S. & Kim, K. –W. (2007). Molecular dynamics study of pattern transfer in nanoimprint lithography, *Tribol. Lett.,* Vol. 25, No. 2, (February 2007) pp. 93-102

MARC : http://www.mscsoftware.com

Okinaka, M.; Tsukagoshi, K. & Aoyagi, Y. (2006). Direct nanoimprint of inorganic-organic hybrid glass, *J. Vac. Sci. Technol. B,* Vol. 24, No. 3, (May 2006) pp. 1402-1404

Song, Z.; Choi, J.; You, B. H.; Lee, J. & Park, S. (2008). Simulation study on stress and deformation of polymeric patterns during the demolding process in thermal imprint lithography, *J. Vac. Sci. Technol. B,* Vol. 26, No. 2, (March 2008) pp. 598-605

Tada, K.; Yasuda, M.; Kimoto, Y.; Kawata, H. & Hirai, Y. (2008). Molecular dynamics study of yield stress of Si mold for nanoimprint lithography, *Jpn. J. Appl. Phys.,* Vol. 47, No. 4, (April 2008) pp. 2320-2323

Tada, K.; Yasuda, M.; Fujii, N.; Kawata, H. & Hirai, Y. (2009a). Molecular dynamics study on mold fracture by nano scale defects in nanoimprint lithography, *Proceedings of 25th European Mask and Lithography Conference*, 32, Dresden, Germany, January 2009

Tada, K.; Kimoto, Y.; Yasuda, M.; Kawata, H. & Hirai, Y. (2009b). Molecular dynamics study of nanoimprint lithography for glass materials, *Jpn. J. Appl. Phys.,* Vol. 48, No. 6, (June 2009) 06FH13

Tada, K.; Yasuda, M.; Kimoto, Y.; Kawata, H. & Hirai, Y. (2009c). Molecular dynamics study on resolution in nanoimprint lithography for glass material, *Mater. Res. Soc. Symp. Proc.*, Vol. 1179, BB06-11, San Francisco, USA, April 2009

Takada, A.; Richet, P.; Catlow, C. R. A. & Price, G. D. (2004). Molecular dynamics simulations of vitreous silica structures, *J. Non-Cryst. Solids,* Vols. 345-346, (October 2004) pp. 224-229

Tersoff, J. (1988a). New empirical approach for the structure and energy of covalent systems, *Phys. Rev. B,* Vol. 37, No. 12, (April 1998) pp. 6991-7000

Tersoff, J. (1988b). Empirical interatomic potential for silicon with improved elastic properties, *Phys. Rev. B,* Vol. 38, No. 14, (November 1998) pp. 9902-9905

Woo, Y. S.; Kim, J. K.; Lee, D. E.; Suh, K. Y. & Lee, W. I. (2007). Density variation of nanoscale patterns in thermal nanoimprint lithography, *Appl. Phys. Lett.,* Vol. 91, No. 25, (December 2007) 253111

Wu, C. -D. & Lin, J. –F. (2008). Multiscale particle dynamics in nanoimprint process, *Appl. Phys. A,* Vol. 91, No. 2 (May 2008) pp. 273-279

Wu, C. -D.; Lin, J. –F. & Fang, T. –H. (2009). Molecular dynamics simulations of the roller nanoimprint process: Adhesion and other mechanical characteristics, *Nanoscale Res. Lett.,* Vol. 4, No. 8 (August 2009) pp. 913-920

Yang, S.; Yu, S. & Cho, M. (2009). Molecular dynamics study to identify mold geometry effect on the pattern transfer in thermal nanoimprint lithography, *Jpn. J. Appl. Phys.,* Vol. 48, No. 6, (June 2009) 06FH03
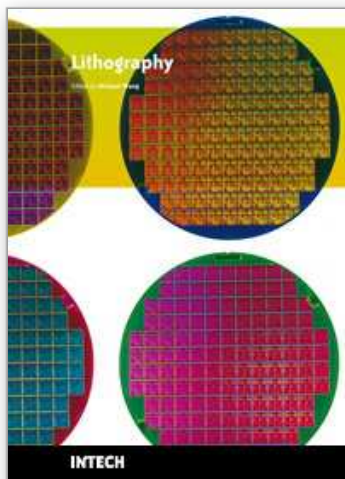
Lithography, the fundamental fabrication process of semiconductor devices, plays a critical role in micro- and nano-fabrications and the revolution in high density integrated circuits. This book is the result of inspirations and contributions from many researchers worldwide. Although the inclusion of the book chapters may not be a complete representation of all lithographic arts, it does represent a good collection of contributions in this field. We hope readers will enjoy reading the book as much as we have enjoyed bringing it together. We would like to thank all contributors and authors of this book.

How to reference

In order to correctly reference this scholarly work, feel free to copy and paste the following:

INTECH

open science | open minds